Title

Hydro-biogeochemical alterations to optical properties of particulate organic matter in the Changjiang Estuary and adjacent shelf area

Authors

Qu, Liyin
Jiao, Ting
Guo, Weidong
et al.

Publication Date

2021-09-01

DOI

10.1016/j.ecolind.2021.107837

Peer reviewed

Ecological Indicators 128 (2021) 107837

Contents lists available at ScienceDirect

Ecological Indicators

journal homepage: www.elsevier.com/locate/ecolind

Hydro-biogeochemical alterations to optical properties of particulate organic matter in the Changjiang Estuary and adjacent shelf area

Liyin Qu [a,1], Ting Jiao [a,1], Weidong Guo [a,b,*], Randy A. Dahlgren [c], Nan Ling [a], Baoyi Feng [a]

[a] State Key Laboratory of Marine Environmental Science, College of Ocean and Earth Sciences, Xiamen University, Xiamen 361102, China
[b] Fujian Provincial Key Laboratory for Coastal Ecology and Environmental Studies, Xiamen University, Xiamen, China
[c] Department of Land, Air and Water Resources, University of California, Davis, USA

ARTICLE INFO

Keywords:
Changjiang Estuary
Base-extracted particulate organic matter
Optical analysis
Pollution tracing
Turbidity maximum zone

ABSTRACT

Base-extracted particulate organic matter (BEPOM) collected in low (spring) and high (summer) runoff seasons in the Changjiang Estuary and adjacent nearshore/offshore shelf areas was examined using absorption and fluorescence spectroscopy. Parallel factor analysis (PARAFAC) identified two humic-like (C1p and C2p) biologically-refractory components and two protein-like (C3p and C4p) bioreactive components. Absorption coefficient *a*350p, C1p and C2p of BEPOM showed strong positive correlations with particulate organic carbon (POC), and were generally higher in spring than in summer. C4p correlated positively with Chl *a*, and was higher in summer than in spring. In the inner estuary, an anthropogenic POM signal from the highly polluted Huangpu River was effectively identified by the fluorescent component ratio $(I_T{:}I_C)_P$. In the nearshore area during spring, resuspension within the well-developed turbidity maximum zone (TMZ) supplied large amounts of refractory POM into the water column. POM fractions from an autochthonous source (i.e., algal bloom) were dominant in the offshore area during the summer. A multivariate regression model inferred that POM export fluxes from the Changjiang River during spring had a higher percentage of labile POM fractions, which were subsequently retained by the TMZ. However, these labile fractions were discharged into the offshore shelf area contributing to hypoxia in the summer. The summer high runoff season also transported large amounts of refractory POM that was subsequently buried in the sediment. This study highlights the utilization of optical analyses to trace pollution sources and reveal POM fate and transport dynamics allowing better assessment of its ecological consequences in estuaries.

1. Introduction

Export of riverine particulate organic matter (POM) to coastal waters represents a key linkage between terrestrial and marine carbon pools (Bianchi, 2011; Remeikaitė-Nikienė et al., 2017; Wang et al., 2012), especially in the case of mega rivers conveying large carbon fluxes (Dagg et al., 2004; López et al., 2012; Spencer et al., 2016). As a dynamic interface between land and ocean, estuaries significantly modify the nature and concentration of riverine POM (Arellano et al., 2019; Bauer et al., 2013; Bianchi et al., 2007). For example, estuarine POM is regulated by several processes, such as particle-solute interactions, *in situ* production/degradation, and sedimentation-resuspension cycles that are especially important in the estuarine turbidity maximum zone (TMZ) (Hermes and Sikes, 2016; Savoye et al., 2012; Yang et al., 2013). Large estuaries are often sites of high population and industrial densities that impart anthropogenic perturbations on estuarine POM dynamics (Canuel and Hardison, 2016; Wang et al., 2020a). Thus, POM contributions from multiple sources, anthropogenic impacts and complex estuarine hydro-biogeochemical dynamics have a strong capacity to alter the properties and fluxes of the POM eventually discharging into coastal waters, thereby modifying the oceanic carbon budget and cycling processes.

Analogous to the measurement of optical properties for colored and fluorescent dissolved organic matter (CDOM and FDOM) (Guo et al., 2014; Qu et al., 2020; Yu et al., 2019), spectral analyses (i.e. absorption and fluorescence) provide an efficient, albeit operationally-defined,

* Corresponding author at: State Key Laboratory of Marine Environmental Science, College of Ocean and Earth Sciences, Xiamen University, Xiamen 361102, China.
E-mail address: wdguo@xmu.edu.cn (W. Guo).
[1] These authors contributed equally to this work.

https://doi.org/10.1016/j.ecolind.2021.107837
Received 2 April 2021; Received in revised form 11 May 2021; Accepted 12 May 2021
Available online 3 June 2021

approach for probing the chemical characteristics of POM through analysis of water- or base-extracted POM (BEPOM) (Brym et al., 2014; Dong et al., 2020; Osburn et al., 2012). Absorption coefficients and spectral slope ($S_{275\text{-}295}$) metrics are valuable proxies for characterizing the concentrations and molecular size of chromophoric POM (CPOM) (Osburn et al., 2012; Yang et al., 2013). Similarly, excitation-emission matrix spectroscopy (EEMs) can reveal several properties of fluorescence POM (FPOM) (Shields et al., 2019). For example, the individual fluorescent components decomposed by parallel factor analysis (PARAFAC) provide valuable information on the quantity, quality and geochemical reactivity of estuarine POM (Lee et al., 2020; Osburn et al., 2015).

The Changjiang Estuary is the largest estuary in China discharging (1.3 ~ 1.5) × 10^{12} g POC per year into the East China Sea (Wang et al., 2012). Abundant runoff and high particle load highlight the role of river-derived POM on the carbon cycle of this turbid estuary (Milliman et al., 1984; Wu et al., 2007). Additionally, the Huangpu River flowing through Shanghai City, a megacity with > 23 million people, experiences chronic anthropogenic pollution leading to high concentrations of nutrients and organic materials that are discharged into the estuary (Guo et al., 2007, 2014). A TMZ is well developed near the mouth area of the Changjiang Estuary resulting in frequent resuspension of bottom sediments in the turbid inshore area that has a significant impact on estuarine carbon dynamics (Zhu et al., 2006). The nutrient-rich waters also contribute to seasonal algal blooms in the offshore shelf area (Wang et al., 2017; Xu et al., 2020). The interaction of these complex factors on POM concentration, properties and reactivity in the Changjiang Estuary has received little study and therefore remains poorly understood.

Herein, we conducted two cruise investigations in the Changjiang Estuary and the adjacent shelf area during spring (low runoff period) and summer (high runoff period) of 2017. The optical properties of BEPOM were characterized and interpreted in combination with associated CDOM, FDOM, particulate organic carbon (POC), chlorophyll *a* (Chl *a*) and nutrient data. The specific aims of this study were: (1) to investigate the spatial and seasonal variations of CPOM/FPOM absorption and fluorescence properties in the Changjiang Estuary; (2) to assess if anthropogenic perturbations on POM properties in the inner estuary can be traced by its optical properties; (3) to reveal the influence of the nearshore TMZ on CPOM/FPOM properties; and (4) to evaluate the bioavailability and ecological consequences of different riverine POM fractions in coastal areas. This study enhances our understanding of natural and anthropogenic impacts on estuarine POM dynamics, thereby improving our knowledge of carbon cycling in river-dominated marginal seas.

2. Materials and methods

2.1. Study area

The Changjiang River (Yangtze River) is the third-longest river in the world with a drainage area of 1.8 × 10^6 km. Multi-year annual export fluxes of freshwater and sediment into the East China Sea are ~ 8.8 × 10^{11} m^3 and 1.27 × 10^8 tons, respectively (Changjiang Sediment Bulletin, 2017). Particulate organic carbon (POC) in the Changjiang River ranges from 0.5 to 2.5% of total suspended matter (Wu et al., 2007). Annual mean temperature and precipitation for the lower Changjiang River are 15.2–15.8 °C and 1149 mm, respectively. As regulated by the East Asian monsoon system, the annual hydrograph of the Changjiang River can be divided into dry (November ~ April; average discharge ~ 20000 m s^{-1}) and wet (May-October; average discharge ~ 40000 m s^{-1}) seasons.

The Changjiang Estuary is a semi-diurnal mesotidal estuary, with an average tidal range of 2.7 m, and is divided into inner estuary, nearshore and offshore shelf areas (Fig. 1). The South Branch (~10–20 km wide, ~20 m depth) of the inner estuary is the main pathway for Changjiang discharge into the East China Sea. Several pollution sources into the South Branch originate from the highly polluted Huangpu River (average discharge of 324 m s^{-1}) and sewage outlets downstream of the Huangpu River (Chai et al., 2006; Guo et al., 2014). Due to shallow depth and strong tidal dynamics, a TMZ persists throughout the year in the fan-shaped nearshore area. High suspended sediment concentrations occur in both surface and bottom layers of the TMZ in the dry season. In contrast, most resuspended sediments are restricted to bottom layers of the TMZ during the wet season (Hua et al., 2020). The offshore shelf is dominated by interactions between Changjiang Diluted Water (CDW) and the northward flowing Taiwan Warm Current (TWC), a branch of the Kuroshio Current characterized by high temperature and salinity (Zhu et al., 2011). During the dry season, CDW flows southeastward and becomes vertically well mixed with the TWC. In the wet season, a stratified CDW plume tends to flow northeastward above the bottom waters from the TWC (Su, 1998). Algal bloom events frequently occur in a winding band along the plume front in the offshore area during spring and summer (Zhou et al., 2020).

2.2. Sample collection and pretreatment

Field observation/collection occurred onboard the R/V *Runjiang I* in the Changjiang Estuary and adjacent continental shelf (120.1 ~ 124.0 °E, 28.8 ~ 32.3 °N) during May 5 ~ 19 and July 20 ~ August 2, 2017, corresponding to spring lower runoff/sediment fluxes (May 2017 sediment: 5.74 × 10^6 tons) and summer higher runoff/sediment fluxes (July 2017 sediment: 28.47 × 10^6 tons) (Fig. 1). Surface water (0.5 m depth) was collected along five land-to-ocean transects at 59 sites, including the

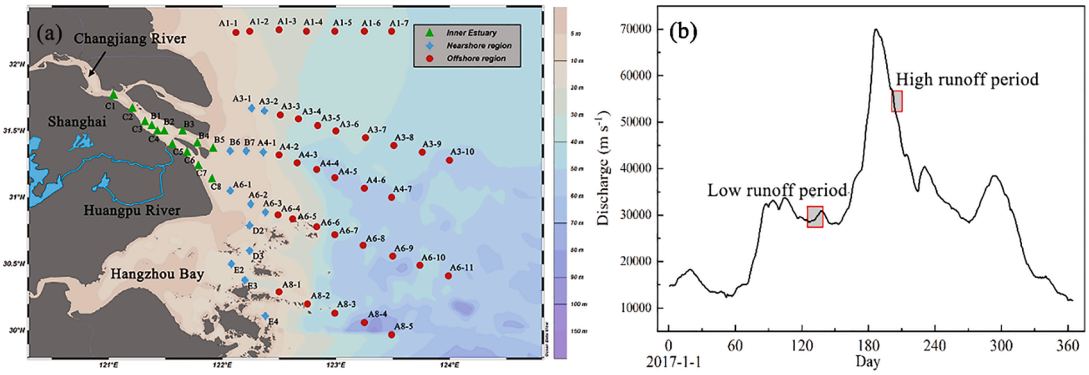

Fig. 1. (a) Sampling stations of the Changjiang Estuary and the adjacent continental shelf; (b) Sampling periods projected on runoff flux curve for the Changjiang River at Datong hydrological station during 2017.

longitudinal C-A6 transect ranging from the inner estuary to the offshore area that covered the entire salinity range of 0–33.4. Water samples were collected using Niskin bottles mounted on a Rosette sampling assembly equipped with calibrated conductivity-temperature-depth (CTD) sensors (SeaBird 911plus, USA). Samples for optical analysis of POM and DOM were filtered immediately through 0.7 μm, pre-combusted (500 °C, 10 h) GF/F filters (Whatman, UK). Filters for base-extractable POM (BEPOM) were stored at −20 °C, while the DOM samples were stored in pre-combusted (500 °C, 5 h) amber glass bottles at 4 °C and measured within one week after returning to the laboratory. To reduce filter background C-contamination, the samples for POC analysis were filtered through 2.2 μm, pre-combusted (650 °C, 10 h) quartz filters (Whatman), which showed comparable POC concentrations to a previous study using 0.7 μm GF/F filters (Zhu et al., 2006). Samples for total suspended matter and Chl *a* were separately filtered through 0.7 μm GF/F filters (Whatman). Filters for Chl *a* were stored in liquid nitrogen until analysis.

2.3. Extraction of BEPOM samples

CPOM and FPOM components of POM were extracted using 15 ml of 0.1 M NaOH solution for 24 h at 4 °C in the dark (Osburn et al., 2012). Extracted solutions were neutralized with concentrated HCl to pH = 7–8, and subsequently filtered through 0.22 μm polyethersulfone filters before CPOM and FPOM analyses.

2.4. Absorption and fluorescence analyses

The absorbance (A_λ) of CPOM and CDOM were scanned using an ultraviolet–visible spectrophotometer (UV-8000, Yuanxi, Shanghai), with Milli-Q water as a blank. The scanning range was 220 to 800 nm at 1-nm intervals. Absorbance spectra were corrected for instrument shift and particle scattering by subtracting absorbance at 700 nm. Absorption coefficients (a_λ) for selected wavelengths and absorption curves were calculated/modeled using the following equations:

$$a_\lambda = 2.303 A_\lambda / l \quad (1)$$

$$a_\lambda = a_{\lambda 0} e^{-S(\lambda - \lambda_0)} \quad (2)$$

The absorption coefficient at 350 nm (a_{350p} for CPOM, a_{350d} for CDOM) was used as a quantitative indicator for CPOM and CDOM abundances, whereas the spectral slope ($S_{275\text{-}295p}$ for CPOM, $S_{275\text{-}295d}$ for CDOM) over the 275–295 nm range was used as a proxy for the average molecular weight of the organic constituents (Brym et al., 2014). Higher $S_{275\text{-}295}$ values usually represent relatively lower molecular weight.

FPOM and FDOM excitation-emission matrix spectra (EEMs) were scanned using a Cary Eclipse spectrophotometer (Varian, Australia). The excitation wavelength range was 240–450 nm with a 5-nm interval, while the emission wavelength range was 280–600 nm with a 2-nm interval. The scanning speed and voltage were 1920 nm/min and 800 V, respectively. All FPOM EEMs were corrected for the volumes of extraction solution and filtered water sample (Osburn et al., 2012). Inner filter effect corrections were not applied as all absorbance data (values ≤ 1.35) were below the threshold value (1.5 in 1-cm cell) for this effect (Kothawala et al., 2013).

A total of 240 EEMs for FPOM and FDOM were modeled by PARAFAC with Matlab 2014b using the DOMfluor toolbox 1.7 (Stedmon and Bro, 2008). EEMs were normalized and blank corrected using Raman normalized Milli-Q water scanned on the same day (Guo et al., 2014). Each PARAFAC component was represented by a maximum fluorescence intensity of F_{max} (R.U, i.e. Raman unit).

2.5. Analysis of chemical and biological parameters

Total suspended matter (TSM) was calculated by dividing the dry particle mass by the filtered water volume. POC concentration was measured using a UNICUBE Trace Elemental Analyzer (Elementar, Germany); samples were pre-acidified to remove inorganic-C (i.e., carbonates) before analysis. Dissolved inorganic nutrients (dissolved inorganic N: DIN = $NH_4 + NO_3 + NO_2$ & soluble reactive P: SRP = PO_4) were measured using an Auto Analyzer 3 (SEAL Analytical, Germany). The Chl *a* concentration was measured using a F-4500 Fluorescence Spectrophotometer (Hitachi, Japan) following the protocol of Jian et al. (2019).

2.6. Data analysis

SPSS 22.0 was used for all statistical analyses (IBM, USA). Figures were generated using Ocean Data View (odv.awi.de) and Origin 2020b (OriginLab, USA). All data are reported as mean ± SD, unless otherwise stated. All "differences" referred to in presentation of the results denote a statistical significant of $p < 0.05$.

3. Results

3.1. Seasonal variation of salinity, TSM, Chl a and POC

The South Branch of the inner Changjiang Estuary was dominated by freshwater (salinity < 1) during both cruises (Fig. 2a, c). The low salinity region spread eastward to the nearshore area during the summer high runoff period, and a widespread CDW plume with salinity < 25 extended in a northeastern direction (Fig. 2c). TSM concentrations in the spring ranged from 0.95 to 1001 mg L^{-1} (80 ± 186 mg L^{-1}), which were significantly higher than those during the summer (10.6–113 mg L^{-1}, 33.9 ± 19.5 mg L^{-1}). High TSM concentrations (472 ± 290 mg L^{-1}) occurred in the wider southern nearshore TMZ in spring (Fig. 2b). The high TSM area became much weaker (87 ± 27 mg L^{-1}) and was isolated to a narrower area between the inner estuary and nearshore area in summer (Fig. 2f).

The distribution of Chl *a* exhibited a similar pattern in both seasons, but was significantly higher in summer (3.2 ± 3.4 μg L^{-1}) versus spring (1.8 ± 1.8 μg L^{-1}) (Fig. 2c, g). Higher Chl *a* concentrations were generally associated with the transitional zone between nearshore and offshore areas having the strongest salinity gradient. POC concentrations in spring and summer were 0.24–8.68 and 0.18–2.46 mg L^{-1}, respectively, with higher POC concentrations in spring (1.28 ± 1.75 mg L^{-1}) versus summer (0.72 ± 0.51 mg L^{-1}). Higher POC concentrations occurred within the nearshore area (3.08 ± 2.76 mg L^{-1}) in spring and within the inner estuary (1.29 ± 0.37 mg L^{-1}) in summer. There was no correlation between POC and Chl *a* in either season (Fig. S1); however, POC was positively correlated with TSM (r: 0.57–0.95) in both seasons.

3.2. Spectral features of CPOM and FPOM

3.2.1. Absorption spectra

Compared with the generally featureless CDOM absorption spectra (Fig. 3d-f), absorption spectra for CPOM had a shoulder peak at 270–280 nm for inner estuary and nearshore TMZ samples (Fig. 3a, b) that became a notable peak in offshore samples (Fig. 3c). This peak, previously reported by (Wang et al., 2020a), is believe to originate from aromatic amino acids (Shick and Dunlap, 2002; Steinberg et al., 2004). The offshore samples also showed weak peaks at ~ 313 and ~ 415 nm (Fig. 3c), which are ascribed to mycosporine-like amino acid and pigment degradation products (Röttgers and Koch, 2012).

3.2.2. Fluorescence spectra and PARAFAC model results

Humic-like fluorescence features of FPOM in the nearshore TMZ were similar to that of FDOM in the same region (Fig. 3h, k). However, the humic-like peaks of FPOM were weaker in the inner estuary and offshore samples than their corresponding FDOM samples (Fig. 3g, i, j, l). In contrast, offshore FPOM samples were dominated by a protein-like peak T (Fig. 3i), similar to fluorescence features of BEPOM in the South Atlantic Bight (Brym et al., 2014).

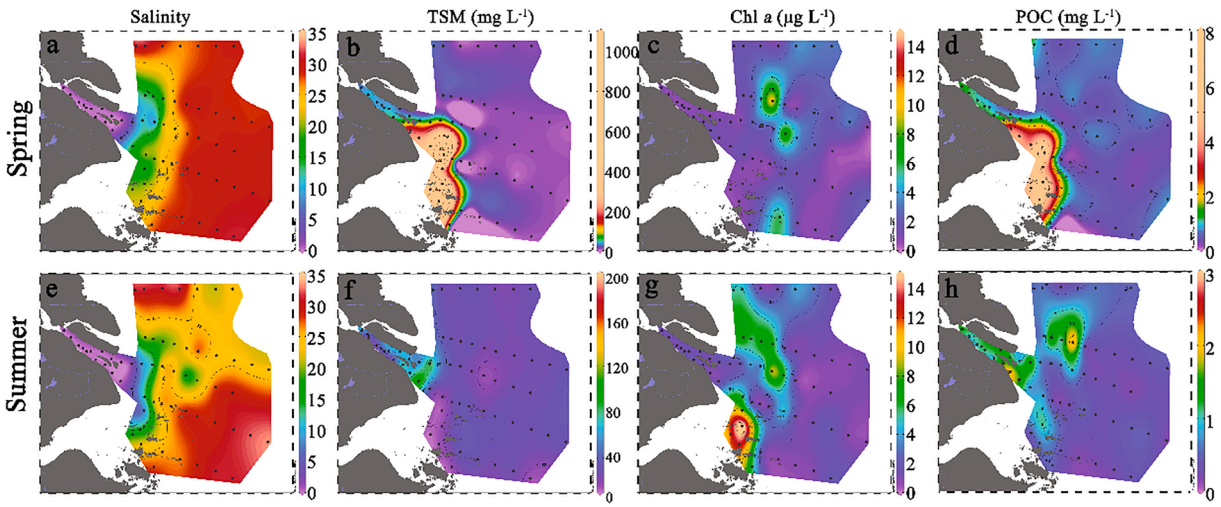

Fig. 2. Distribution of salinity, TSM, Chl *a* and POC in the Changjiang Estuary and adjacent shelf area during the spring (low flow) and summer (high flow) cruises of 2017.

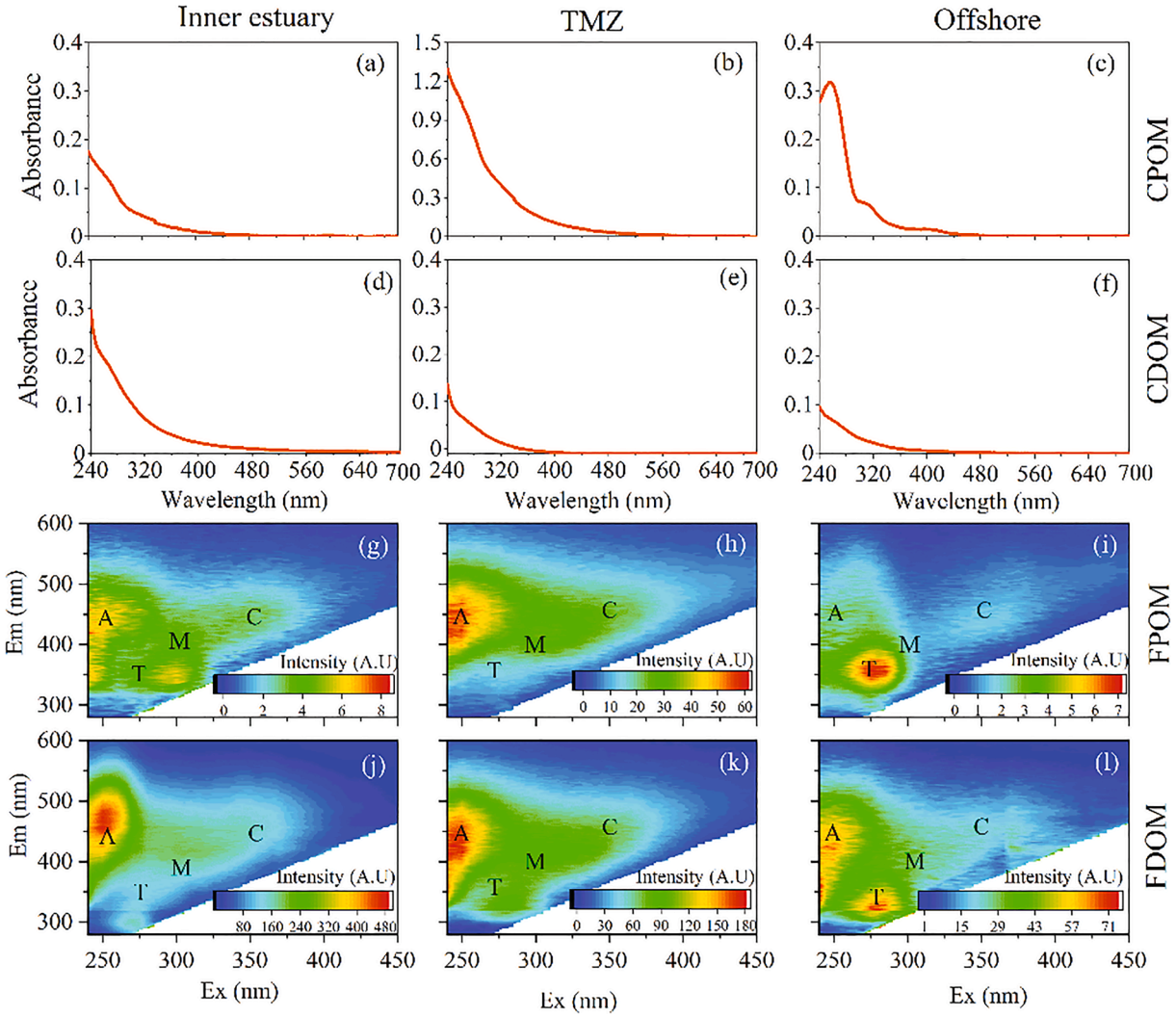

Fig. 3. Corrected absorption and fluorescence spectra for BEPOM and DOM in spring 2017. Salinities of inner estuary, nearshore and offshore areas were 0, 21.3 and 30.0, respectively. Peak A: Ex/Em = 250/450 nm, peak M: Ex/Em = 300/400 nm, peak C: 350/450 nm, peak T: 275/350 nm.

Four PARAFAC components (C1-C4) were identified for FPOM and FDOM (Fig. S2). Component C1 (240, 315/412 nm) was spectrally similar to component C5 (240, 310/426 nm) identified in BEPOM samples from the North River Estuary (North Carolina, USA) and attributed to fresh terrestrial humic substances (Osburn et al., 2015). Component C2 (255, 365/456 nm) matched component C1 (250, 345/447 nm) of BEPOM samples from the subtropical Minjiang River (Fujian Province, China) (Wang et al., 2020a), which was ascribed to terrestrial humic components sourced from soils (Osburn et al., 2015). Component C3 (240, 280/332 nm) represents a ubiquitous protein-like component, consistent with a combination of tryptophan-like and tyrosine-like fluorophores (Wei et al., 2019). Component C4 (275/356 nm) was spectrally similar to the tryptophan-like peak T originating from biological sources (Wang et al., 2020b).

3.3. Temporal and spatial variation of optical properties for BEPOM

The *a*350p, C1p and C2p properties of BEPOM demonstrated a strong positive correlation with POC (r: 0.67–0.93) and negative correlation with $S_{275\text{-}295}$p (r: 0.52–0.72) during the two sampling periods (Fig. S1). Thus, these parameters had similar distribution patterns across high and low runoff periods (Fig. 4a, c, f, h). An independent *t*-test demonstrated that these parameters were significantly higher in spring versus summer in the nearshore area. However, there was no seasonally significant difference in the inner estuary and offshore area. C3p values showed a moderate correlation with POC (r: 0.62–0.72), and were significantly higher in spring versus summer, especially in the inner estuary and nearshore area. C4p values were not correlated to other CPOM/FPOM components, but were positively correlated with Chl *a* (r: 0.61–0.71). C4p values were higher in summer versus spring and were highest in the offshore area in both seasons.

The $(I_T{:}I_C)_p$ ratio represents the fluorescence intensity ratio of protein-like: humic-like (C3:C2) components of FPOM. The ratio was highest below the Huangpu River outlet during the spring period (Fig. 5a); an area also having elevated particulate (C3p) and dissolved protein-like ($C3_d$, Guo et al., 2014) components and a high $(I_T{:}I_C)_d$ ratio (Fig. 5a). During the summer, the $(I_T{:}I_C)_p$ ratio gradually decreased from the inner estuary to the offshore area, with no obvious peak value below the Huangpu River outlet (Fig. 5b).

The spC1p and spC2p parameters are the specific fluorescence of C1p and C2p relative to POC concentrations. Both parameters were generally higher in the inner estuary and offshore area compared to the nearshore area (Fig. 5c, d). In spring, spC1p and spC2p were elevated below the Huangpu River outlet and then quickly decreased in the TMZ (Fig. 5c). The spC3 values in spring were high below the Huangpu River outlet and the offshore area, but conversely showed a consistent decrease from the inner estuary to the offshore area during the summer (Fig. 5c, d). The longitudinal distribution of spC4p was similar in both seasons, with low values in the inner estuary and nearshore area and a large increase within the offshore area (Fig. 5c, d).

3.4. Temporal and spatial distribution of optical properties of DOM

CDOM (a350d) absorption coefficients generally decreased with increasing salinity in both spring and summer seasons, but with the highest values observed below the Huangpu River outlet (Fig. 4k, p). The CDOM spectral slope ($S_{275\text{-}295}$d) showed contrasting spatial variations (Fig. 4i, q) that were consistent with our previous studies in the same estuary (Guo et al., 2007, 2014). The a355d and $S_{275\text{-}295}$d values for the freshwater end-member of the Changjiang Estuary in spring 2017 (1.89 ± 0.02 m^{-1}, 0.0174 ± 0.0004 m^{-1}) were similar to our previous investigation in spring 2011 (1.72 ± 0.09 m^{-1}, 0.0176 ± 0.0002 m^{-1}) (Guo et al., 2014). However, the a355d for the freshwater end-member in summer 2017 (1.50 ± 0.23 m^{-1}), which was similar to that measured

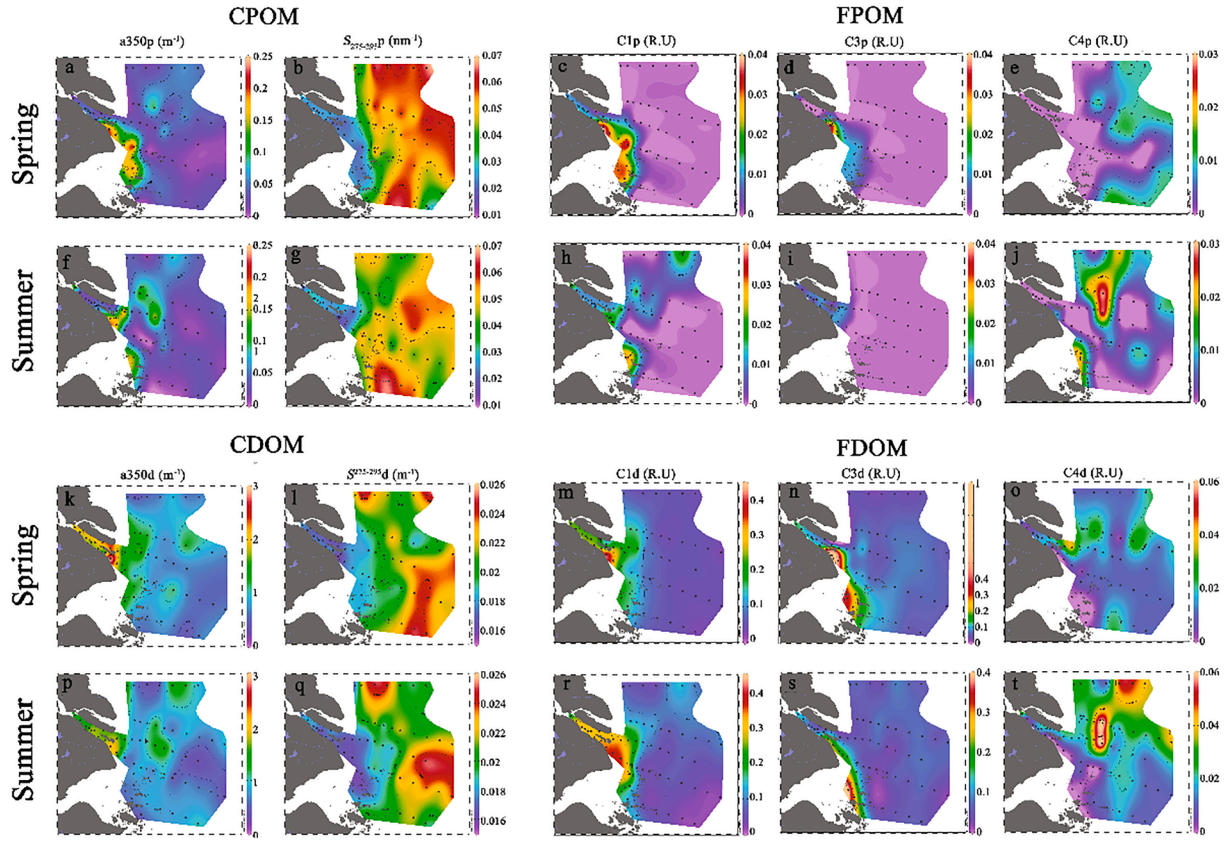

Fig. 4. Temporal and spatial distribution of optical properties for POM (a-h) and DOM (i-p) during the spring (low flow) and summer (high flow) seasons. Note the strong correlations between components C2p and C1p and components C2d and C1d (see Fig. S1).

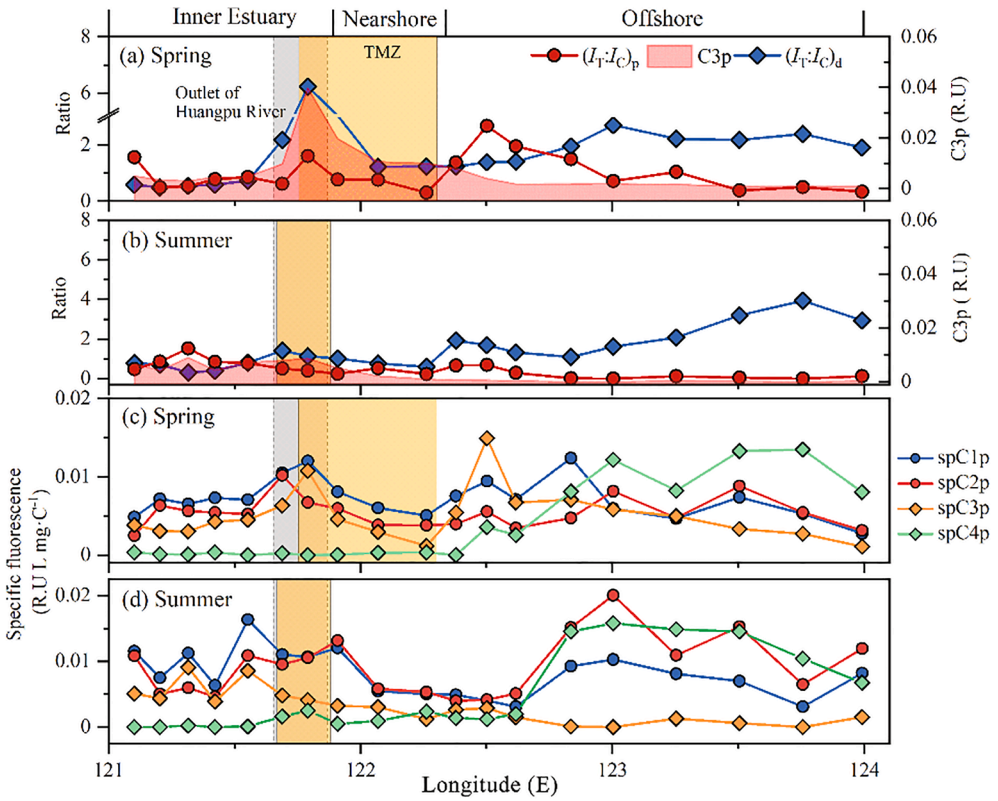

Fig. 5. Changes in I_T:I_C ratios of FPOM and FDOM, C3p and specific fluorescence of PARAFAC components of FPOM along longitudinal C-A6 transect (see Fig. 1) from the inner estuary to the offshore area.

in summer 2003 (1.45 ± 0.17 m^{-1}), was lower than that recorded in summer 2011 (2.66 ± 0.05 m^{-1}). The $S_{275\text{-}295}$d in summer 2017 (0.0180 ± 0.0007 nm^{-1}) was higher than that observed in summer 2011 (0.0164 ± 0.0002 nm^{-1}) (Guo et al., 2007, 2014). There were no seasonal differences in a350d or $S_{275\text{-}295}$d in the offshore area. The a350d and $S_{275\text{-}295}$d showed negative and positive correlations, respectively, with salinity in both seasons ($p < 0.05$).

The C1d and C2d fluorescence components were significantly correlated with a350d (r: 0.64–0.87) during both seasons, thereby demonstrating similar seasonal patterns with a350d, and negatively correlated with salinity (0.91–0.95) (Fig. 5m, n, r, s). The C3d was weakly correlated with salinity and Chl *a* (r < 0.3), and showed much higher values in the nearshore TMZ. The C4d showed no significant correlation with salinity or Chl *a* in the overall estuary-coastal continuum, but its values were generally highest in the offshore area, especially in summer (Fig. 5o, t).

4. Discussion

The optical properties of BEPOM and DOM demonstrated significant spatial and seasonal variations along the estuary-coast continuum of the Changjiang Estuary (Figs. 2–5). To reveal the specific regional dynamics of BEPOM in the inner estuary, nearshore and offshore areas of this continuum, three separate (i.e., area specific) principal component analyses (PCA) were applied using all particulate/dissolved organic, nutrients, TSM and Chl *a* parameters (Fig. 6). The first two principal components (PC1 and PC2) of each model explained 61.9, 57.9 and 57.9% of the variations, respectively.

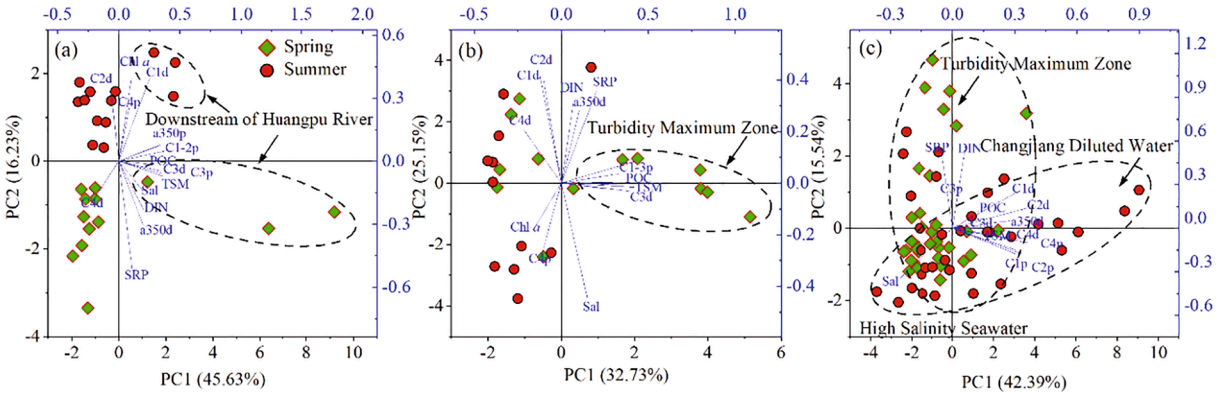

Fig. 6. PCA analysis for quantitative POM, DOM and water quality parameters during the spring (May) low runoff and summer (July) high runoff seasons: (a) inner estuary, (b) nearshore area, and (c) offshore area. Dots and diamonds represent the sampling sites during the spring and summer seasons, respectively.

4.1. $(I_T{:}I_C)_p$ ratio: A BEPOM tracer of anthropogenic perturbation on estuarine POM dynamics

In the inner estuary, PC1 explained 45.6% of data variance (Fig. 6a). Samples downstream of the Huangpu River outlet (St. C6-C8) grouped along the positive axis of PC1 in both seasons. These samples had high loadings on particulate (C3p) and dissolved (C3d) protein-like components, as well as nutrients (DIN and SRP). Fluorescence ratios of $(I_T{:}I_C)_p$ and $(I_T{:}I_C)_d$ and specific fluorescence of C3p (spC3p) also showed peak values for these highly polluted stations (Fig. 5). The Huangpu River and associated sewage outlets export large amounts of anthropogenic pollutants from domestic, industrial and agricultural activities into the South Branch (Guo et al., 2014; Zhang et al., 2021). Notably, the estimated input flux of protein-like components from the Huangpu River was as high as 33.6–81.9% of the total export flux of protein-like components for the Changjiang River Estuary (Guo et al., 2014). Thus, we infer that PC1 represents a pollution signal, and the $(I_T{:}I_C)_p$ ratio of BEPOM may be used as a sensitive tracer for anthropogenic perturbation on estuarine POM dynamics from municipal, industrial and agricultural sources.

Summer (July) samples had lower positive PC1 scores than in spring (May) samples (Fig. 6a). Conversely, the summer samples had higher positive PC2 scores and high loadings for terrestrial C1d and C2d signals (Coble, 2007; Li et al., 2015). These dynamics suggest that anthropogenic perturbations of POM in the inner estuary were diluted by an increase of terrestrial POM inputs during the summer high runoff period. Furthermore, high loadings of Chl *a* and protein-like C4p on the positive PC2 axis indicate POM contributions from phytoplankton production in the summer season.

4.2. Regulation of estuarine POM dynamics by TMZ processes in the nearshore area

In the nearshore area, PC1 explained 32.7% of the total variance (Fig. 6b). TMZ samples from the nearshore area showed a higher score on the positive PC1 axis in spring. Humic-like C1p and C2p, protein-like C3p and C3d, TSM and POC had higher loadings on the positive axis of PC1 and were closely related to TMZ samples. In the shallow nearshore TMZ zone of the Changjiang Estuary, sediment resuspension by tidal pumping can reach as high as 66.5–88.5% (Zhang et al., 2021). Previous studies found that sediments generally have high levels of relatively refractory BEPOM humic-like C1, C2 and dissolved protein-like C3 components (Hur et al., 2014). A recent study of DOM from bottom samples in the TMZ zone of the Changjiang Estuary also provides optical and molecular evidence that the suspended sediment contained a large amount of organic matter with condensed aromatic structures (Zhou et al., 2021). This infers that the addition of POM/DOM from sediment resuspension in the TMZ zone is an important source of refractory organic matter (Yang et al., 2013). For humic-like components, preferential adsorption and aggregation of dissolved constituents to particles and limitation of POM photodissolution at the turbidity maximum zone may additionally contribute to the high levels of C1p and C2p (Liu and Shank, 2015; Zhou et al., 2021). However, the lower specific fluorescence of C1p-C3p (spC1-C3p) suggests that the resuspended POM has lower FPOM features/properties (Fig. 5).

The high protein-like C3p component in TMZ samples could be sourced from upstream portions of the Huangpu River watershed (Fig. 4d). Both protein-like components C3p and C3d showed a 23.7–30.7% decrease after passing through the TMZ (Fig. 4d), suggesting that attached and free-living bacteria in the TMZ can degrade labile organic matter (Servais and Garnier, 2006). This microbial degradation process may also be responsible for the high level of the humic-like C1p component, being a transformation product of the C3p and C3d components (Osburn et al., 2015).

PC2 explained 25.2% of the total variance. The summer samples distributed along both positive and negative axes. The positive axis was related to terrestrial signals of humic-like C1d and C2d, whereas the negative axis was related to planktonic signals of Chl *a* and protein-like C4p. This implies that estuarine mixing processes were an important regulating factor for POM dynamics in the surface nearshore area following weaken of the TMZ during the summer high runoff period. Thus, the intensity of the TMZ, as regulated by river flow, is an important factor controlling POM dynamics in the Changjiang Estuary.

4.3. Biological and photochemical influences on offshore POM dynamics

In the offshore area, PC1 and PC2 explained 42.4% and 15.5% of the total variation, respectively (Fig. 6c). The summer samples distributed along the PC1 axis. Samples influenced by the CDW aligned along the positive PC1 axis, with high loadings from C1p, C2p, C1d, C2d and C4p. During the summer high runoff period, the CDW contained a large amount of particulate and dissolved terrestrial humic-like C1 and C2 components along with nutrients (Guo et al., 2007, 2014; Qu et al., 2019). The supply of nutrients supported the patchy distribution of algal blooms (Chl *a*: 9.7–17.0 μg L^{-1}) in the diluted waters during the summer. This primary production contributed to the high levels of fresh autochthonous particulate and dissolved tryptophan-like C4 component (Osburn et al., 2015; Shields et al., 2019). This interpretation is consistent with previous biological and isotopic evidence that demonstrated the POC in the offshore area was characteristic of a phytoplankton source (Wang et al., 2017, 2016). In addition, the lower C1d in the offshore region during spring could be due to photodegradation along the transport pathway (Fig. 4) (Alling et al., 2010). On the contrary, the higher C1d in the offshore region during summer coupled with high C1p suggest that this component could source from photodissolution of riverine exported POM (Liu and Shank 2015).

Summer samples aligned along the negative PC1 axis were from the southeast offshore area (Fig. 6c). This area showed an overlapping of spring and summer samples along the negative PC2 axis, suggesting that organic matter properties exhibited small seasonal variations in this offshore area dominated by the Taiwan Warm Current. Spring samples aligning in the positive PC2 direction were located near the TMZ and displayed high loadings of terrestrial protein-like C3p and nutrients (DIN and SRP) indicative of a riverine source (Fig. 6c).

4.4. Ecological consequences of POM export with contrasting bioavailability/bioreactivity

The fate of terrestrial POM discharging into coastal ecosystems largely depends on its composition and bioavailability. POM components sourced from soil or weathered materials are usually refractory in nature (i.e. resistant to microbial decomposition during transport), and thus tend to be ultimately buried with sediments in shelf areas (Wang et al., 2012). On the contrary, recently produced fresh POM is more biologically labile (i.e., bioreactive) and thus plays an active role in coastal biogeochemistry and foodweb dynamics (Shields et al., 2019; Wang et al., 2016). Therefore, distinguishing riverine export fluxes of POM with different bioavailability from major river sources is critical for understanding its ecological consequences in coastal areas (Arellano et al., 2019; Bianchi et al., 2007).

A multivariate regression model was used to estimate the POC content of freshwater samples (salinity = 0) represented by each FPOM component during both the spring and summer seasons (Osburn et al., 2015). To avoid multicollinearity issues caused by autocorrelation among the fluorescent components, the correlated components were combined to establish the regression model. Further, the *F*max of each fluorescence component was scaled up by 50% to match the average recovery of BEPOC to total POC (Brym et al., 2014; Osburn et al., 2015). The resulting empirical model was POC = 23.39 × (C1 + C2 + C3) + 0.44 ($R^2 = 0.86$, $p < 0.01$) for the spring cruise, and POC = 9.76 × (C1 + C2) + 7.87 × C3 + 67.70 × C4 + 0.80 ($R^2 = 0.68$, $p < 0.01$) for the summer cruise. The specific POC flux for each fluorescent component

having contrasting bioavailability/bioreactive properties are listed in Table 1. The constant term in this empirical model corresponds to the non-base extractable POM fraction and can be classified as highly refractory POM. In contrast, protein-like C3 and C4 components represent relatively labile components with higher bioavailability (Guo et al., 2014). The POC flux for each component during the spring and summer seasons was then computed by multiplying the specific POC content of the TSM by the sediment flux for the corresponding season.

The POC flux of degradable protein-like C3p and C4p components had a higher percentage in spring (18.6%) versus summer (11.3%, Table 1), inferring that POM in the spring season was more bioreactive than POM in the summer (Osburn and Bianchi, 2016; Wang et al., 2020a). However, the absolute flux values were similar in both seasons due to a much higher sediment flux during the summer high runoff period (Table 1). Degradation of these bioreactive components will contribute to deoxygenation processes in the adjacent shelf area, thereby contributing to seasonal hypoxia. In spring, these labile components were mainly retained/transformed within the TMZ, thus contributing to oxygen consumption within the nearshore area. The retention/removal rate of C3p was ~ 78% based on flux differences between the entrance (C7) and outlet (E4 and A8-1) of the TMZ. In summer, hypoxia events (DO < 2 mg L^{-1}) frequently occur in the shelf area close to the Changjiang Estuary (Wang et al., 2017, 2016; Zhu et al., 2011), including the northern part of the offshore area during our summer investigation (Fig. S3). As the labile POM flux discharges into this shelf area as part of its transport with enhanced summer Changjiang Diluted Water flows, the degradation of the riverine labile POM may contribute to hypoxia as the POM settles to the bottom water layer and surface sediments. Higher nutrient concentrations in summer contribute to enhanced primary productivity with decaying algal biomass further contributing to oxygen demand.

The POC flux of refractory components had both a higher percentage and absolute flux in summer (62.4%, 3.78×10^{11} g C) versus spring (28.7%, 1.00×10^{11} g C) (Table 1). These results indicate that discharge of the refractory POC fraction from the Changjiang River into the coastal area dominantly occurs in the wet season that generates higher river flows. Humic-like components C2 and C1 are considered relatively refractory (Osburn et al., 2012, 2015). These components may largely persist during riverine transport and subsequently settle into the coastal sediments (Fig. 4h). The persistence of these humic components within the accumulated sediments during early diagenesis warrants further study as their fate will play an important role in the global C cycle.

5. Conclusions

Absorption and fluorescence analyses of base-extracted POM collected during low (spring) and high (summer) runoff seasons revealed distinct spatial and seasonal variations in POM dynamics within the Changjiang Estuary and adjacent shelf area. In the inner estuary, an anthropogenic POM signal from the highly polluted Huangpu River and sewage discharge outlets were distinguished based on the $(I_T{:}I_C)_P$ ratio, especially in spring. These labile POM fractions were largely removed by the well-developed turbidity maximum zone in the nearshore area, where considerable sediment resuspension also supplied large amounts of relatively refractory POM into the water column. In contrast, the labile POM fractions in summer were discharged to the offshore shelf area by the elevated Changjiang Diluted Water flux. The algal growth stimulated by riverine nutrient inputs to the offshore shelf area also contribute to a dominance of autochthonous POM fractions in summer. Both sources of labile POM fractions could contribute to hypoxia in this region. The summer season also transported large amounts of refractory POM fractions that we posit become buried in the sediment serving as a C sink within the global C cycle. This study highlights that optical analyses of base-extractable POM enhance our understanding of the fate and transport of POM in estuarine and coastal ecosystems.

Table 1
Riverine POC component fluxes and their percentage contribution to the entire POM fraction exported into the Changjiang Estuary during spring (low runoff) and summer (high runoff) seasons (Units = 10^{11} g C).

	Spring		Summer	
	Flux	Percentage	Flux	Percentage
Microbial, Terrestrial (C1) POC	1.05	29.9%	0.90	14.8%
Soil, Terrestrial (C2) POC	0.80	22.8%	0.70	11.5%
Anthropogenic, Fresh (C3) POC POPOC	0.66	18.6%	0.36	5.9%
Planktonic (C4) POC	<0.01	<0.1%	0.33	5.4%
Soil; Non-fluorescence POC	1.00	28.7%	3.78	62.4%
Total predicted POC	**3.52**	**100%**	**6.07**	**100%**
Total measured POC	**3.60**	—	**6.07**	—

CRediT authorship contribution statement

Liyin Qu: Writing - original draft, Writing - review & editing. **Ting Jiao:** Investigation, Formal analysis. **Weidong Guo:** Conceptualization, Funding acquisition, Review. **Randy A. Dahlgren:** Writing - review & editing. **Nan Ling:** Investigation. **Baoyi Feng:** Investigation.

Declaration of Competing Interest

The authors declare that they have no known competing financial interests or personal relationships that could have appeared to influence the work reported in this paper.

Acknowledgements

This work was jointly supported by the National Natural Science Foundation of China and Fujian Province (U1805241) and the National Natural Science Foundation of China (41876083). The authors are grateful to the captain, crew, technicians and scientists aboard the R/V *Runjiang I* for their assistance during the cruises (NORC2017-04). The authors thank Linjie Huang, Lei Wu, Wen Shi and Cheng Jin for sample collection and analyses. Total suspended sediments, dissolved oxygen and chlorophyll *a* data were shared by research groups of Dr. Fenfen Zhang (East China Normal University), Dr. Weidong Zhai (Shandong University) and Dr. Guipeng Yang (Ocean University of China).

Appendix A. Supplementary data

Supplementary data to this article can be found online at https://doi.org/10.1016/j.ecolind.2021.107837.

References

Alling, V., Sanchez-Garcia, L., Porcelli, D., Pugach, S., Vonk, J.E., van Dongen, B., Mörth, C.-M., Anderson, L.G., Sokolov, A., Andersson, P., Humborg, C., Semiletov, I., Gustafsson, Ö., 2010. Nonconservative behavior of dissolved organic carbon across the Laptev and East Siberian seas. Global Biogeochem. Cy. 24 (4).

Arellano, A.R., Bianchi, T.S., Osburn, C.L., D'Sa, E.J., Ward, N.D., Oviedo-Vargas, D., Joshi, I.D., Ko, D.S., Shields, M.R., Kurian, G., Green, J., 2019. Mechanisms of organic matter export in estuaries with contrasting carbon sources. J. Geophys. Res.-Biogeo. 124 (10), 3168–3188.

Bauer, J.E., Cai, W.-J., Raymond, P.A., Bianchi, T.S., Hopkinson, C.S., Regnier, P.A.G., 2013. The changing carbon cycle of the coastal ocean. Nature 504 (7478), 61–70.

Bianchi, T.S., 2011. The role of terrestrially derived organic carbon in the coastal ocean: A changing paradigm and the priming effect. P. Natl. Acad. Sci. U.S.A. 108 (49), 19473–19481.

Bianchi, T.S., Wysocki, L.A., Stewart, M., Filley, T.R., McKee, B.A., 2007. Temporal variability in terrestrially-derived sources of particulate organic carbon in the lower Mississippi River and its upper tributaries. Geochim. Cosmochim. Acta 71 (18), 4425–4437.

Brym, A., Paerl, H.W., Montgomery, M.T., Handsel, L.T., Ziervogel, K., Osburn, C.L., 2014. Optical and chemical characterization of base-extracted particulate organic matter in coastal marine environments. Mar. Chem. 162, 96–113.

Canuel, E.A., Hardison, A.K., 2016. Sources, ages, and alteration of organic matter in Estuaries. Annu. Rev. Mar. Sci. 8 (1), 409–434.

Chai, C., Yu, Z., Song, X., Cao, X., 2006. The status and characteristics of eutrophication in the Yangtze River (Changjiang) estuary and the adjacent East China Sea, China. Hydrobiologia 563 (1), 313–328.
Coble, P.G., 2007. Marine optical biogeochemistry: the chemistry of ocean color. Chem. Rev. 107, 402–418.
Dagg, M., Benner, R., Lohrenz, S., Lawrence, D., 2004. Transformation of dissolved and particulate materials on continental shelves influenced by large rivers: plume processes. Cont. Shelf Res. 24 (7-8), 833–858.
Dong, Y., Li, Y., Kong, F., Zhang, J., Xi, M., 2020. Source, structural characteristics and ecological indication of dissolved organic matter extracted from sediments in the primary tributaries of the Dagu River. Ecol. Ind. 109, 105776. https://doi.org/10.1016/j.ecolind.2019.105776.
Guo, W., Stedmon, C.A., Han, Y., Wu, F., Yu, X., Hu, M., 2007. The conservative and non-conservative behavior of chromophoric dissolved organic matter in Chinese estuarine waters. Mar. Chem. 107 (3), 357–366.
Guo, W., Yang, L., Zhai, W., Chen, W., Osburn, C.L., Huang, X., Li, Y., 2014. Runoff-mediated seasonal oscillation in the dynamics of dissolved organic matter in different branches of a large bifurcated estuary: the Changjiang Estuary. J. Geophys. Res.-Biogeo. 119 (5), 776–793.
Hermes, A.L., Sikes, E.L., 2016. Particulate organic matter higher concentrations, terrestrial sources and losses in bottom waters of the turbidity maximum, Delaware Estuary, USA. Estuar. Coast. Shelf. S. 180, 179–189.
Hua, X., Huang, H., Wang, Y., Yu, X., Zhao, K., Chen, D., 2020. Seasonal Estuarine turbidity maximum under strong tidal dynamics: three-year observations in the Changjiang River Estuary. Water 12, 1854–1872.
Hur, J., Lee, B.-M., Shin, K.-H., 2014. Spectroscopic characterization of dissolved organic matter isolates from sediments and the association with phenanthrene binding affinity. Chemosphere 111, 450–457.
Jian, S., Zhang, H.-H., Yang, G.-P., Li, G.-L., 2019. Variation of biogenic dimethylated sulfur compounds in the Changjiang River Estuary and the coastal East China Sea during spring and summer. J. Mar. Syst. 199, 103222.
Kothawala, D.N., Murphy, K.R., Stedmon, C.A., Weyhenmeyer, G.A., Tranvik, L.J., 2013. Inner filter correction of dissolved organic matter fluorescence: correction of inner filter effects. Limnol. Oceanogr.-Meth. 11, 616–630.
Lee, M.-H., Lee, S.Y., Yoo, H.-Y., Shin, K.-H., Hur, J., 2020. Comparing optical versus chromatographic descriptors of dissolved organic matter (DOM) for tracking the non-point sources in rural watersheds. Ecol. Ind. 117, 106682.
Li, P., Chen, L., Zhang, W., Huang, Q., Mao, J., 2015. Spatiotemporal distribution, sources, and photobleaching imprint of dissolved organic matter in the Yangtze Estuary and its adjacent sea using fluorescence and parallel factor analysis. PLoS One 10 (6), e0130852.
Liu, Q., Shank, G.C., 2015. Solar radiation-enhanced dissolution (photodissolution) of particulate organic matter in Texas estuaries. Estuar. Coast. 38 (6), 2172–2184.
López, R., Del Castillo, C.E., Miller, R.L., Salisbury, J., Wisser, D., 2012. Examining organic carbon transport by the Orinoco River using SeaWiFS imagery. J. Geophys. Res.-Biogeo. 117. G03022.
Milliman, J.D., Xie, Q.C., Yang, Z.S., 1984. Transfer of Particulate Organic-Carbon and Nitrogen from the Yangtze-River to the Ocean. Am. J. Sci. 284, 824–834.
Osburn, C.L., Bianchi, T.S., 2016. Editorial: linking optical and chemical properties of dissolved organic matter in natural waters. Front. Mar. Sci. 3, 3.
Osburn, C.L., Handsel, L.T., Mikan, M.P., Paerl, H.W., Montgomery, M.T., 2012. Fluorescence tracking of dissolved and particulate organic matter quality in a river-dominated Estuary. Environ. Sci. Technol. 46 (16), 8628–8636.
Osburn, C.L., Mikan, M.P., Etheridge, J.R., Burchell, M.R., Birgand, F., 2015. Seasonal variation in the quality of dissolved and particulate organic matter exchanged between a salt marsh and its adjacent estuary. J. Geophys. Res.-Biogeo. 120 (7), 1430–1449.
Qu, L.Y., Wu, Y.F., Li, Y., Stubbins, A., Dahlgren, R.A., Chen, N.W., Guo, W.D., 2020. El Nino-driven dry season flushing enhances dissolved organic matter export from a subtropical watershed. Geophys. Res. Lett. 47 e2020GL089877.
Qu, D., Yu, H., Sun, Y., Zhao, Y., Wei, Q., Yu, H., Kelly, R.M., Yuan, Y., 2019. Numerical study on the summertime patches of red tide in the adjacent sea of the Changjiang (Yangtze) River Estuary, China. Mar. Pollut. Bull. 143, 242–255.
Remeikaitė-Nikienė, N., Lujanienė, G., Malejevas, V., Barisevičiūtė, R., Zilius, M., Vybernaitė-Lubienė, I., Garnaga-Budrė, G., Stankevičius, A., 2017. Assessing nature and dynamics of POM in transitional environment (the Curonian Lagoon, SE Baltic Sea) using a stable isotope approach. Ecol. Ind. 82, 217–226.
Röttgers, R., Koch, B.P., 2012. Spectroscopic detection of a ubiquitous dissolved pigment degradation product in subsurface waters of the global ocean. Biogeosciences 9 (7), 2585–2596.
Savoye, N., David, V., Morisseau, F., Etcheber, H., Abril, G., Billy, I., Charlier, K., Oggian, G., Derriennic, H., Sautour, B., 2012. Origin and composition of particulate organic matter in a macrotidal turbid estuary: The Gironde Estuary, France. Estuar. Coast. Shelf. S. 108, 16–28.
Servais, P., Garnier, J., 2006. Organic carbon and bacterial heterotrophic activity in the maximum turbidity zone of the Seine estuary (France). Aquat. Sci. 68 (1), 78–85.
Shick, J.M., Dunlap, W.C., 2002. Mycosporine-like amino acids and related gadusols: biosynthesis, accumulation, and UV-protective functions in aquatic organisms. Annu. Rev. Physiol. 64 (1), 223–262.
Shields, M.R., Bianchi, T.S., Osburn, C.L., Kinsey, J.D., Ziervogel, K., Schnetzer, A., Corradino, G., 2019. Linking chromophoric organic matter transformation with biomarker indices in a marine phytoplankton growth and degradation experiment. Mar. Chem. 214, 103665.
Spencer, R.G.M., Hernes, P.J., Dinga, B., Wabakanghanzi, J.N., Drake, T.W., Six, J., 2016. Origins, seasonality, and fluxes of organic matter in the Congo River. Global Biogeochem. Cy. 30 (7), 1105–1121.
Stedmon, C.A., Bro, R., 2008. Characterizing dissolved organic matter fluorescence with parallel factor analysis: a tutorial. Limnol. Oceanogr.-Meth. 6 (11), 572–579.
Steinberg, D.K., Nelson, N.B., Carlson, C.A., Prusak, A., 2004. Production of chromophoric dissolved organic matter (CDOM) in the open ocean by zooplankton and the colonial cyanobacterium Trichodesmium spp. Mar. Ecol. Prog. Ser. 267, 45–56.
Su, J., 1998. Circulation dynamics of the China Seas north of 188N, in edited by A. R. Robinson, and K. H. Brink. Wiley & Sons Inc, New York.
Wang, B., Chen, J., Jin, H., Li, H., Huang, D., Cai, W.-J., 2017. Diatom bloom-derived bottom water hypoxia off the Changjiang estuary, with and without typhoon influence. Limnol. Oceanogr. 62 (4), 1552–1569.
Wang, H., Dai, M., Liu, J., Kao, S.-J., Zhang, C., Cai, W.-J., Wang, G., Qian, W., Zhao, M., Sun, Z., 2016. Eutrophication-Driven Hypoxia in the East China Sea off the Changjiang Estuary. Environ. Sci. Technol. 50 (5), 2255–2263.
Wang, H., Li, Z., Zhuang, W.-E., Hur, J., Yang, L., Wang, Y., 2020a. Spectral and isotopic characteristics of particulate organic matter in a subtropical estuary under the influences of human disturbance. J. Mar. Syst. 203, 103264.
Wang, X., Ma, H., Li, R., Song, Z., Wu, J., 2012. Seasonal fluxes and source variation of organic carbon transported by two major Chinese Rivers: the Yellow River and Changjiang (Yangtze) River. Global Biogeochem. Cy. 26 (2).
Wang, H., Wang, Y., Zhuang, W.-E., Chen, W., Shi, W., Zhu, Z., Yang, L., 2020b. Effects of fish culture on particulate organic matter in a reservoir-type river as revealed by absorption spectroscopy and fluorescence EEM-PARAFAC. Chemosphere 239, 124734.
Wei, M., Gao, C., Zhou, Y., Duan, P., Li, M., 2019. Variation in spectral characteristics of dissolved organic matter in inland rivers in various trophic states, and their relationship with phytoplankton. Ecol. Ind. 104, 321–332.
Wu, Y., Zhang, J., Liu, S.M., Zhang, Z.F., Yao, Q.Z., Hong, G.H., Cooper, L., 2007. Sources and distribution of carbon within the Yangtze River system. Estuar. Coast. Shelf. S. 71 (1-2), 13–25.
Xu, L.J., Yang, D.Z., Greenwood, J., Feng, X.R., Gao, G.D., Qi, J.F., Cui, X., Yin, B.S., 2020. Riverine and oceanic nutrients govern different algal bloom domain near the Changjiang Estuary in Summer. J. Geophys. Res.-Biogeo. 125 e2020JG005727.
Yang, L., Guo, W., Hong, H., Wang, G., 2013. Non-conservative behaviors of chromophoric dissolved organic matter in a turbid estuary: roles of multiple biogeochemical processes. Estuar. Coast. Shelf. S. 133, 285–292.
Yu, X., Zhang, J., Kong, F., Li, Y., Li, M., Dong, Y., Xi, M., 2019. Identification of source apportionment and its spatial variability of dissolved organic matter in Dagu River-Jiaozhou Bay estuary based on the isotope and fluorescence spectroscopy analysis. Ecol. Ind. 102, 528–537.
Zhang, J., Du, Y.N., Zhang, G.S., Chang, Y., Zhou, Y.C., Zhang, Z.F., Wu, Y., Chen, J.W., Zhang, A.Y., Zhu, Z.Y., Liu, S.M., 2021. Increases in the seaward river flux of nutrients driven by human migration and land-use changes in the tide-influenced delta. Sci. Total Environ. 761, 144501.
Zhou, F., Chai, F., Huang, D.J., Wells, M., Ma, X., Meng, Q.C., Xue, H.J., Xuan, J.L., Wang, P.B., Ni, X.B., Zhao, Q., Liu, C.G., Su, J.L., Li, H.L., 2020. Coupling and decoupling of high biomass phytoplankton production and hypoxia in a highly dynamic coastal system: the Changjiang (Yangtze River) Estuary. Front. Mar. Sci. 7, 259.
Zhou, Y.P., He, D., He, C., Li, P.H., Fan, D.D., Wang, A.Y., Zhang, K., Chen, B.S., Zhao, C., Wang, Y.T., Shi, Q., Sun, Y.G., 2021. Spatial changes in molecular composition of dissolved organic matter in the Yangtze River Estuary: implications for estuarine carbon cycling. Sci. Total Environ. 759, 143531.
Zhu, Z.Y., Zhang, J., Wu, Y., Lin, J., 2006. Bulk particulate organic carbon in the East China Sea: Tidal influence and bottom transport. Prog Oceanogr 69 (1), 37–60.
Zhu, Z.-Y., Zhang, J., Wu, Y., Zhang, Y.-Y., Lin, J., Liu, S.-M., 2011. Hypoxia off the Changjiang (Yangtze River) estuary: oxygen depletion and organic matter decomposition. Mar. Chem. 125 (1-4), 108–116.